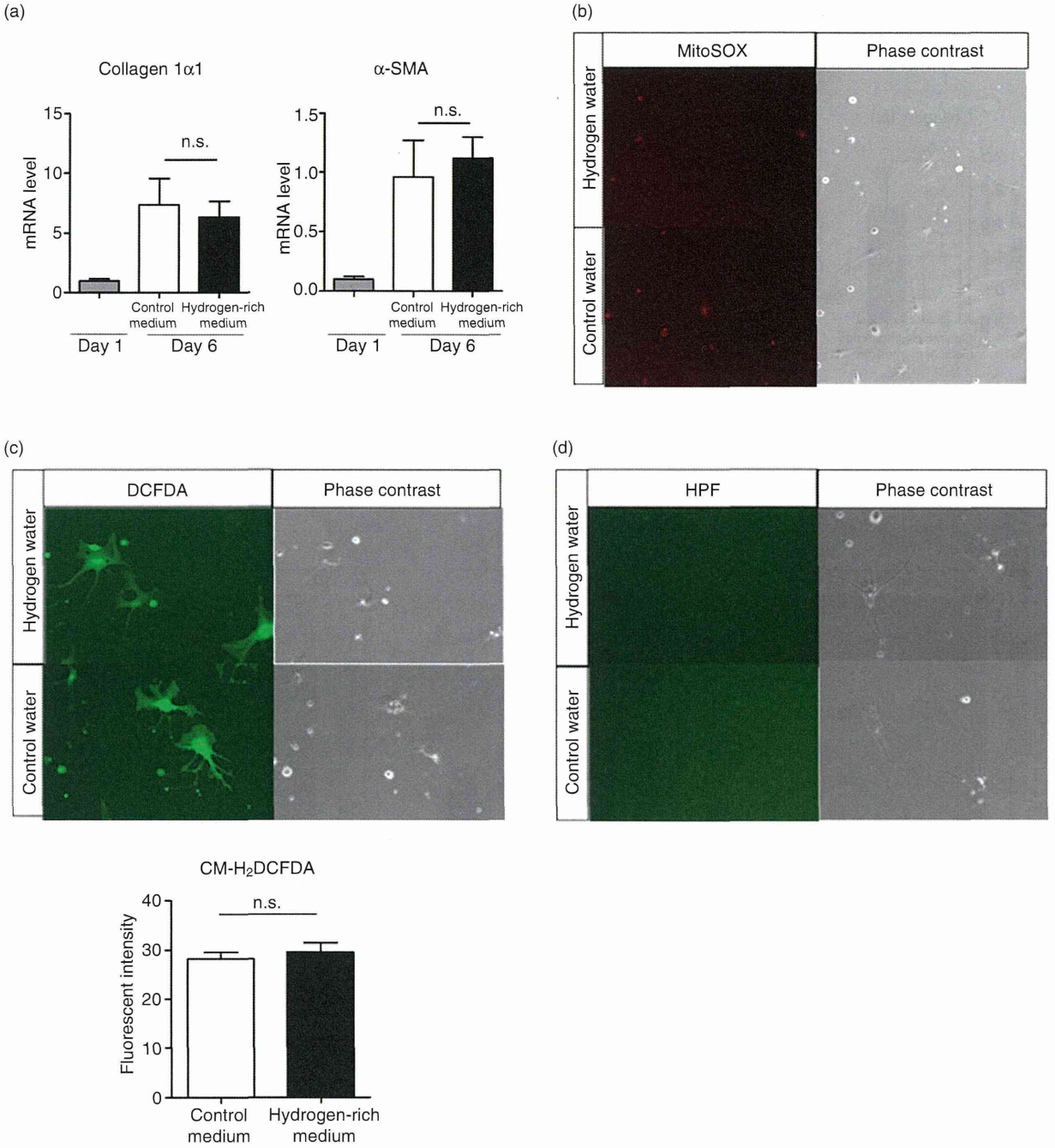


**Figure 7** Hydrogen-rich medium does not suppress the activation of cultured hepatic stellate cells (HSC). HSC were isolated from C57BL/6 mice and cultured with or without hydrogen-rich medium for 5 days on plastic dishes to allow activation. Hydrogen-rich medium did not suppress the increase in the mRNA levels of HSC activation markers (collagen1α1 and α-smooth muscle actin [α-SMA]) (a). The HSC showed faint signals of $O^{\cdot}{}_{2^-}$, as detected by MitoSOX (b). HSC activated on plastic dishes showed the production of $H_2O_2$, as detected by 2′,7′-dichlorodihydrofluorescein (CM-$H_2$DCFDA) (c), but culturing in hydrogen-rich medium did not show any suppressive effect on $H_2O_2$ production (c). The HSC did not show the presence of $OH^{\cdot}$, as detected by hydroxyphenyl fluorescein (HPF) staining (d).

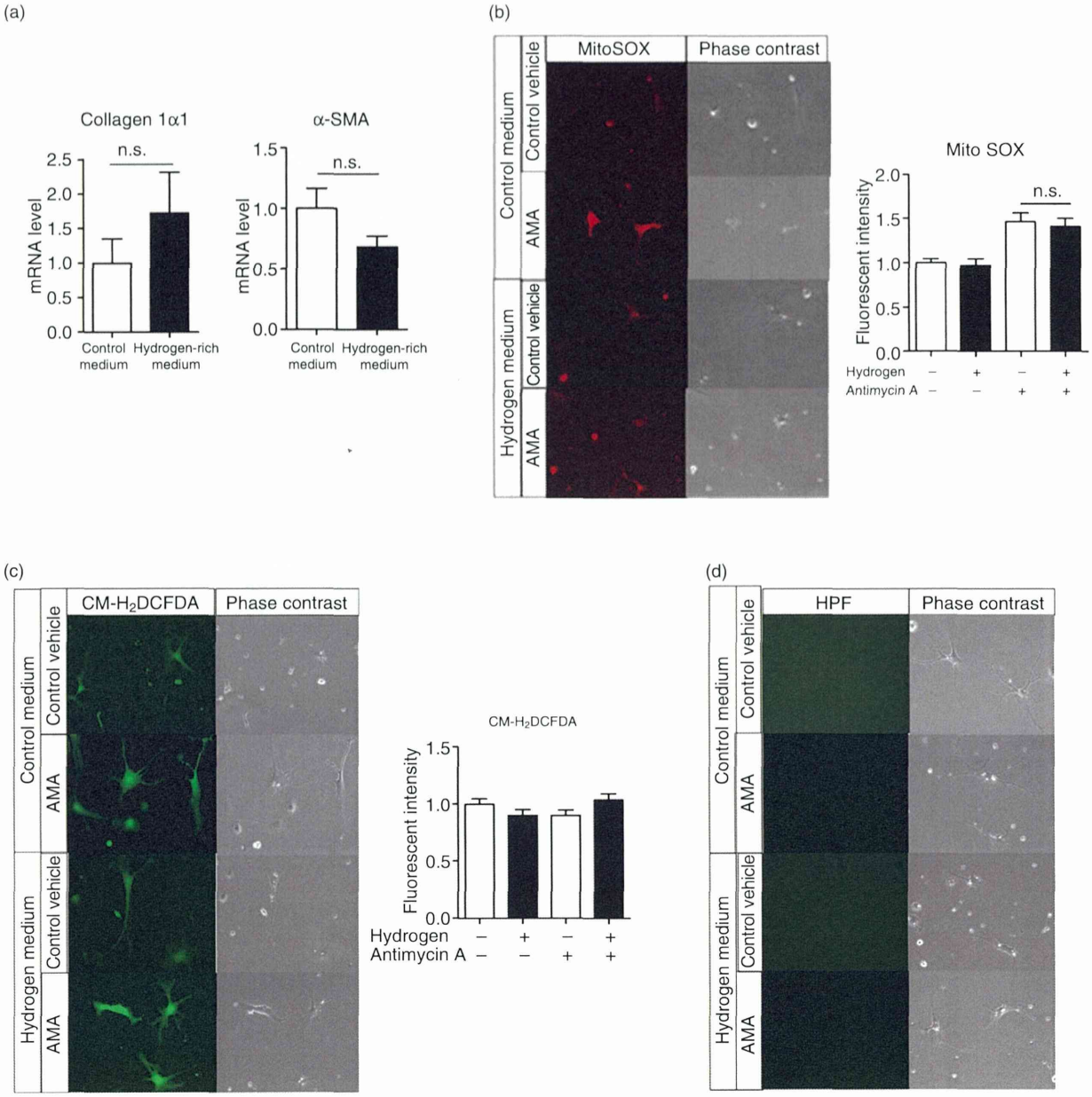


**Figure 8** Hydrogen-rich medium does not suppress or accelerate the hepatic stellate cell (HSC) activation induced by antimycin A (AMA) treatment. Isolated HSC were cultured with or without hydrogen-rich medium in the presence of AMA to assess the effect of hydrogen on HSC activation under excess oxidative stress. Culturing in hydrogen-rich medium did not affect the mRNA expression levels of HSC activation markers (collagen1α1 and α-smooth muscle actin [α-SMA]) (a). Although AMA stimulation increased the intracellular level of $O_{\cdot 2^-}$ as detected by MitoSOX (b), culturing in hydrogen-rich medium did not suppress this increase in the $O_{\cdot 2^-}$ level. The $H_2O_2$ level, as detected by 2′,7′-dichlorodihydrofluorescein (CM-$H_2$DCFDA), was not altered by AMA stimulation (c). Moreover, we could not detect intracellular OH· even under stimulation with AMA (d).

## DISCUSSION

IN THE PRESENT study, we investigated whether orally ingested $H_2$-water suppressed liver fibrogenesis. Our study demonstrated that $H_2$-water showed antifibrogenic effects in the $CCl_4$ and TAA models but did not show any difference in the BDL model. $H_2$-water exhibited an OH·-scavenging effect in the $CCl_4$ and TAA model; however, in the BDL model, OH· was not detected in the liver even in the control water group. We suggest that the antifibrotic effect of $H_2$-water is associated with the scavenging of OH·.

Carbon tetrachloride and TAA have been widely used to induce injury in experimental models of liver fibrosis. In both these models, ROS play a crucial role in the development of liver fibrosis.[22,23] Intracellular ROS usually refers to the excess amounts of $O\cdot_{2^-}$, $H_2O_2$ and OH·. Among them, OH· is the strongest ROS and reacts indiscriminately with nucleic acids, lipids and proteins.[10] To date, many reports have described the antifibrotic effect of antioxidants.[24–26] However, the mechanisms by which antioxidants suppress liver fibrosis, and the particular ROS that forms the primary target for antioxidants, remain to be elucidated. Galli *et al.* described the proliferation and invasiveness of HSC by $O\cdot_{2^-}$ induced by the action of xanthine and xanthine oxidase.[5] Therefore, we first sought to determine whether $H_2$-water exerted its antifibrotic effect through the suppression of $O\cdot_{2^-}$ production. The results of our *in vitro* experiments, however, indicated that the hydrogen-rich medium did not influence the $O\cdot_{2^-}$ and the $H_2O_2$ levels in both HSC and hepatocytes. We examined the expression of $O\cdot_{2^-}$ in the injured liver by staining freshly frozen liver sections with MitoSOX, and the results showed that $H_2$-water does not influence the $O\cdot_{2^-}$ levels in the liver (data not shown). Instead, we found that oral ingestion of $H_2$-water resulted in the suppression of OH· levels in the liver and that hydrogen-rich medium attenuated the generation of OH· in cultured hepatocytes. These results indicated that OH· is the primary target for $H_2$-water.

It is well known that peroxynitrite is a reactive oxidant produced from nitric oxide and superoxide. $O\cdot_{2^-}$ may react with nitric oxide, which could be generated constitutively from sinusoidal endothelial cell-derived nitric oxide synthase. Aram *et al.* reported that necrosis and liver fibrosis induced by CCl4 administration were decreased in inducible nitric oxide synthase deficient mice.[27] We examined 3-nitrotyrosine in the liver. Hydrogen water did not show significant effect on 3-nitrotyrosine generation in the liver. Hydrogen seems to have less effect on peroxynitrite.

With regard to the target cells of ROS in the liver, many studies have implicated oxidative stress in the activation and proliferation of HSC and hence in the development of liver fibrosis.[28,29] However, other studies have shown conflicting data as to the effects of ROS on HSC proliferation and viability.[6] Our study did not show any signs of OH· production when HSC are activated by culturing on plastic dishes. This result indicates hydrogen does not influence HSC activation directly.

On the other hand, $H_2$-water suppressed hepatocyte death, as demonstrated by inhibition of transaminase release in the $H_2$-water group. Hepatocyte injuries stimulate the phagocytosis of dead hepatocytes by Kupffer cells.[30] Activated Kupffer cells secrete profibrogenic cytokines such as TGF-β-1, which activate HSC and eventually lead to liver fibrogenesis.[31] Our *in vivo* study showed the decreased expression of TGF-β1 mRNA. Decreased induction of TGF-β1, a particularly potent profibrogenic cytokine, may be a key factor in alleviation of the fibrogenic response by $H_2$-water. Expression of α-SMA, an indicator for HSC activation, was also inhibited by intake of $H_2$-water, suggesting that inhibition of TGF-β1 induction results in reduced activation of HSC, which leads to reduced collagen deposition. Taken together, we presume that $H_2$-water suppresses triggering profibrogenic response by scavenging hydroxyl radicals that induce hepatocyte death and subsequent activation of Kupffer cells, TGF-β1 induction and HSC activation.

We did not detect any suppressive effect of $H_2$-water on fibrogenesis in BDL model. This differential effect of $H_2$-water on liver fibrosis caused by varying causes is interesting. This difference may be explained by the variation in the initial step triggering the inflammatory response in the two models: hepatocyte injury triggers the fibrotic pathway in hepatotoxin models, whereas biliary epithelial cell injury is the primary step triggering fibrosis in the BDL model. Therefore, the absence of the antifibrotic effect of $H_2$-water in the BDL model seems to be concordant with the hepatoprotective properties of $H_2$-water. Moreover, considering our results that indicate $H_2$-water selectively scavenges OH·, the difference can be explained by the variation of ROS contribution in the models: hepatocyte injuries by $CCl_4$ and TAA are OH·-dependent injuries, whereas biliary injury by BDL is independent of OH·.

Recent studies have demonstrated that $H_2$ reduces OH· and may have potential for widespread medical application as a novel, safe and effective antioxidant

with minimal adverse effects.[32] Elimination of OH· is biologically important because although $O\cdot_{2}^{-}$ and $H_2O_2$ are detoxified by the antioxidant defense enzymes superoxide dismutase and peroxidase or glutathione peroxidase, no enzyme detoxifies OH·.[11]

The systemic distribution of $H_2$ after oral intake of $H_2$-water has been described previously by Kamimura *et al.*[33] They monitored the dynamic movement of hydrogen in rat liver after p.o. administration of $H_2$-water by introducing a needle-type hydrogen sensor into the liver. They showed that oral intake of $H_2$-water helps maintain a sufficient hydrogen concentration in the liver for 1 h. Further, $H_2$-water has already been applied in humans. Clinical trials have revealed that supplementation with $H_2$-water reduced oxidative stress in patients with type 2 diabetes[34] and those with potential metabolic syndrome,[35] thereby indicating that it influenced glucose[34] and cholesterol metabolism.[35] These findings indicate that $H_2$-water can be administrated safely to humans and has potential for use as an antifibrotic agent.

In conclusion, $H_2$-water protects hepatocytes from injury by scavenging OH· and thereby suppresses liver fibrogenesis in mice.

## ACKNOWLEDGMENTS

THIS STUDY WAS supported by Grants-in-Aid for Scientific Research (no. 23659647, 23390322 and 21791248) from Japan Society for the Promotion of Science (JSPS). We thank Dr Akiko Taura and Dr Rie Horie for technical assistance and for providing the protocol to dissolve hydrogen into cell culture medium.

## REFERENCES

1 Albanis E, Friedman SL. Hepatic fibrosis. Pathogenesis and principles of therapy. *Clin Liver Dis* 2001; **5**: 315–34.
2 Bataller R, Brenner DA. Hepatic stellate cells as a target for the treatment of liver fibrosis. *Semin Liver Dis* 2001; **21**: 437–51.
3 Dooley S, ten Dijke P. TGF-beta in progression of liver disease. *Cell Tissue Res* 2012; **347**: 245–56.
4 Parola M, Robino G. Oxidative stress-related molecules and liver fibrosis. *J Hepatol* 2001; **35**: 297–306.
5 Galli A, Svegliati-Baroni G, Ceni E *et al.* Oxidative stress stimulates proliferation and invasiveness of hepatic stellate cells via a MMP2-mediated mechanism. *Hepatology* 2005; **41**: 1074–84.
6 Dunning S, Hannivoort RA, de Boer JF, Buist-Homan M, Faber KN, Moshage H. Superoxide anions and hydrogen peroxide inhibit proliferation of activated rat stellate cells and induce different modes of cell death. *Liver Int* 2009; **29**: 922–32.
7 Chinopoulos C, Adam-Vizi V. Calcium, mitochondria and oxidative stress in neuronal pathology. Novel aspects of an enduring theme. *FEBS J* 2006; **273**: 433–50.
8 Turrens JF. Mitochondrial formation of reactive oxygen species. *J Physiol* 2003; **552**: 335–44.
9 Sauer H, Wartenberg M, Hescheler J. Reactive oxygen species as intracellular messengers during cell growth and differentiation. *Cell Physiol Biochem* 2001; **11**: 173–86.
10 Halliwell B. Oxidants and human disease: some new concepts. *FASEB J* 1987; **1**: 358–64.
11 Ohsawa I, Ishikawa M, Takahashi K *et al.* Hydrogen acts as a therapeutic antioxidant by selectively reducing cytotoxic oxygen radicals. *Nat Med* 2007; **13**: 688–94.
12 Sun H, Chen L, Zhou W *et al.* The protective role of hydrogen-rich saline in experimental liver injury in mice. *J Hepatol* 2011; **54**: 471–80.
13 Taura K, Miura K, Iwaisako K *et al.* Hepatocytes do not undergo epithelial-mesenchymal transition in liver fibrosis in mice. *Hepatology* 2010; **51**: 1027–36.
14 Popov Y, Sverdlov DY, Sharma AK *et al.* Tissue transglutaminase does not affect fibrotic matrix stability or regression of liver fibrosis in mice. *Gastroenterology* 2011; **140**: 1642–52.
15 Taura A, Kikkawa YS, Nakagawa T, Ito J. Hydrogen protects vestibular hair cells from free radicals. *Acta Otolaryngol Suppl* 2010; **(563)**: 95–100.
16 Tamaki N, Hatano E, Taura K *et al.* CHOP deficiency attenuates cholestasis-induced liver fibrosis by reduction of hepatocyte injury. *Am J Physiol Gastrointest Liver Physiol* 2008; **294**: G498–505.
17 Weiskirchen R, Gressner AM. Isolation and culture of hepatic stellate cells. *Methods Mol Med* 2005; **117**: 99–113.
18 Iwaisako K, Hatano E, Taura K *et al.* Loss of Sept4 exacerbates liver fibrosis through the dysregulation of hepatic stellate cells. *J Hepatol* 2008; **49**: 768–78.
19 Tomizawa S, Imai H, Tsukada S *et al.* The detection and quantification of highly reactive oxygen species using the novel HPF fluorescence probe in a rat model of focal cerebral ischemia. *Neurosci Res* 2005; **53**: 304–13.
20 Setsukinai K, Urano Y, Kakinuma K, Majima HJ, Nagano T. Development of novel fluorescence probes that can reliably detect reactive oxygen species and distinguish specific species. *J Biol Chem* 2003; **278**: 3170–5.
21 Lopez-De Leon A, Rojkind M. A simple micromethod for collagen and total protein determination in formalin-fixed paraffin-embedded sections. *J Histochem Cytochem* 1985; **33**: 737–43.
22 Masuda Y. [Learning toxicology from carbon tetrachloride-induced hepatotoxicity]. *Yakugaku Zasshi* 2006; **126**: 885–99.
23 Stankova P, Kucera O, Lotkova H, Rousar T, Endlicher R, Cervinkova Z. The toxic effect of thioacetamide on rat liver in vitro. *Toxicol In Vitro* 2010; **24**: 2097–103.

24 Szuster-Ciesielska A, Plewka K, Daniluk J, Kandefer-Szerszen M. Betulin and betulinic acid attenuate ethanol-induced liver stellate cell activation by inhibiting reactive oxygen species (ROS), cytokine (TNF-alpha, TGF-beta) production and by influencing intracellular signaling. *Toxicology* 2011; **280:** 152–63.
25 Ohyama T, Sato K, Kishimoto K *et al.* Azelnidipine is a calcium blocker that attenuates liver fibrosis and may increase antioxidant defence. *Br J Pharmacol* 2012; **165:** 1173–87.
26 Paik YH, Yoon YJ, Lee HC *et al.* Antifibrotic effects of magnesium lithospermate B on hepatic stellate cells and thioacetamide-induced cirrhotic rats. *Exp Mol Med* 2011; **43:** 341–9.
27 Aram G, Potter JJ, Liu X, Torbenson MS, Mezey E. Lack of inducible nitric oxide synthase leads to increased hepatic apoptosis and decreased fibrosis in mice after chronic carbon tetrachloride administration. *Hepatology* 2008; **47:** 2051–8.
28 Paik YH, Iwaisako K, Seki E *et al.* The nicotinamide adenine dinucleotide phosphate oxidase (NOX) homologues NOX1 and NOX2/gp91(phox) mediate hepatic fibrosis in mice. *Hepatology* 2011; **53:** 1730–41.
29 Li J, Fan R, Zhao S *et al.* Reactive oxygen species released from hypoxic hepatocytes regulates MMP-2 expression in hepatic stellate cells. *Int J Mol Sci* 2011; **12:** 2434–47.
30 Canbay A, Feldstein AE, Higuchi H *et al.* Kupffer cell engulfment of apoptotic bodies stimulates death ligand and cytokine expression. *Hepatology* 2003; **38:** 1188–98.
31 Gressner AM, Bachem MG. Molecular mechanisms of liver fibrogenesis – a homage to the role of activated fat-storing cells. *Digestion* 1995; **56:** 335–46.
32 Terasaki Y, Ohsawa I, Terasaki M *et al.* Hydrogen therapy attenuates irradiation-induced lung damage by reducing oxidative stress. *Am J Physiol Lung Cell Mol Physiol* 2011; **301:** L415–426.
33 Kamimura N, Nishimaki K, Ohsawa I, Ohta S. Molecular hydrogen improves obesity and diabetes by inducing hepatic FGF21 and stimulating energy metabolism in db/db mice. *Obesity (Silver Spring)* 2011; **19:** 1396–403.
34 Kajiyama S, Hasegawa G, Asano M *et al.* Supplementation of hydrogen-rich water improves lipid and glucose metabolism in patients with type 2 diabetes or impaired glucose tolerance. *Nutr Res* 2008; **28:** 137–43.
35 Nakao A, Toyoda Y, Sharma P, Evans M, Guthrie N. Effectiveness of hydrogen rich water on antioxidant status of subjects with potential metabolic syndrome-an open label pilot study. *J Clin Biochem Nutr* 2010; **46:** 140–9.

# Origin of myofibroblasts in the fibrotic liver in mice

Keiko Iwaisako[a,b,c,1], Chunyan Jiang[a,c,d,1], Mingjun Zhang[a,1], Min Cong[a,c,d], Thomas Joseph Moore-Morris[e], Tae Jun Park[a], Xiao Liu[a,c], Jun Xu[a,c], Ping Wang[a,c,d], Yong-Han Paik[f], Fanli Meng[a,g], Masataka Asagiri[h], Lynne A. Murray[i], Alan F. Hofmann[a], Takashi Iida[j], Christopher K. Glass[k], David A. Brenner[a], and Tatiana Kisseleva[c,2]

Departments of [a]Medicine, [c]Surgery, and [k]Cellular and Molecular Medicine, and [e]School of Pharmacy, University of California, San Diego, La Jolla, CA 92093; [b]Department of Target Therapy Oncology, Graduate School of Medicine, Kyoto University, Kyoto 606-8507, Japan; [d]Beijing Friendship Hospital, Capital Medical University, Beijing 100050, China; [f]Division of Gastroenterology and Hepatology, Department of Internal Medicine, Samsung Medical Center, Sungkyunkwan University School of Medicine, Seoul 135-710, Korea; [g]Department of Hepatology, Qilu Hospital Shandong University, Shandong 250012, China; [h]Innovation Center for Immunoregulation and Therapeutics, Graduate School of Medicine, Kyoto University, Kyoto 606-8507, Japan; [i]MedImmune Ltd., Cambridge CB21 6GH, United Kingdom; and [j]Department of Chemistry, College of Humanities and Sciences, Nihon University, Sakurajousui, Setagaya, Tokyo 156-8550, Japan

Edited* by Michael Karin, University of California, San Diego School of Medicine, La Jolla, CA, and approved June 23, 2014 (received for review January 6, 2014)

**Hepatic myofibroblasts are activated in response to chronic liver injury of any etiology to produce a fibrous scar. Despite extensive studies, the origin of myofibroblasts in different types of fibrotic liver diseases is unresolved. To identify distinct populations of myofibroblasts and quantify their contribution to hepatic fibrosis of two different etiologies, collagen-α1(I)-GFP mice were subjected to hepatotoxic (carbon tetrachloride; $CCl_4$) or cholestatic (bile duct ligation; BDL) liver injury. All myofibroblasts were purified by flow cytometry of $GFP^+$ cells and then different subsets identified by phenotyping. Liver resident activated hepatic stellate cells (aHSCs) and activated portal fibroblasts (aPFs) are the major source (>95%) of fibrogenic myofibroblasts in these models of liver fibrosis in mice. As previously reported using other methodologies, hepatic stellate cells (HSCs) are the major source of myofibroblasts (>87%) in $CCl_4$ liver injury. However, aPFs are a major source of myofibroblasts in cholestatic liver injury, contributing >70% of myofibroblasts at the onset of injury (5 d BDL). The relative contribution of aPFs decreases with progressive injury, as HSCs become activated and contribute to the myofibroblast population (14 and 20 d BDL). Unlike aHSCs, aPFs respond to stimulation with taurocholic acid and IL-25 by induction of collagen-α1(I) and IL-13, respectively. Furthermore, BDL-activated PFs express high levels of collagen type I and provide stimulatory signals to HSCs. Gene expression analysis identified several novel markers of aPFs, including a mesothelial-specific marker mesothelin. PFs may play a critical role in the pathogenesis of cholestatic liver fibrosis and, therefore, serve as an attractive target for antifibrotic therapy.**

ECM deposition | markers of fibrogenic myofibroblasts

Chronic liver injury of many etiologies results in liver fibrosis. There are two general types of chronic liver diseases, hepatocellular (injury to hepatocytes, such as chronic viral hepatitis and nonalcoholic steatohepatitis) and cholestatic (obstruction to bile flow, such as primary biliary cirrhosis and primary sclerosing cholangitis) (1). Experimental rodent models of liver fibrosis mimic these two types of chronic liver injuries: Repeated carbon tetrachloride ($CCl_4$) administration produces hepatocelluar injury, and common bile duct ligation (BDL) produces cholestatic injury (2). In all chronic liver diseases, myofibroblasts are embedded in the fibrous scar and are the source of this excessive extracellular matrix (ECM). Myofibroblasts, which are not present in normal liver, are characterized by distinct morphology, contractility with intracellular stress fibers [α-smooth muscle actin (α-SMA), nonmuscle myosin, and vimentin], and secretion of extracellular matrix (fibronectin and fibrillar collagens) (1, 2).

The cells of origin of hepatic myofibroblasts are unresolved, and perhaps the fibrosis induced by different types of liver injury results from different fibrogenic cells. Hepatic myofibroblasts may originate from bone marrow (BM)-derived mesenchymal cells and fibrocytes, but only a small contribution of BM-derived cells to the myofibroblast population has been detected in experimental liver fibrosis (3–5). Another potential source of myofibroblast is epithelial-to-mesenchymal transition (EMT), in which epithelial cells acquire a mesenchymal phenotype and may give rise to fully differentiated myofibroblasts. However, recent cell fate mapping studies have failed to detect any hepatic myofibroblasts originating from hepatocytes, cholangiocytes, or epithelial progenitor cells (3, 6–10). Thus, the major sources of myofibroblasts in liver fibrosis are the endogenous liver mesenchymal cells, which consist of portal fibroblasts and hepatic stellate cells.

Quiescent hepatic stellate cells (qHSCs) are located in the space of Disse, store retinoids in lipid droplets, and express neural markers, such as glial fibrillary acidic protein (GFAP), synaptophisin, and nerve growth factor receptor p75 (1). In response to injury, qHSCs down-regulate vitamin A-containing lipid droplets and neural markers, and differentiate into α-SMA–expressing myofibroblasts (1, 2). Portal fibroblasts normally comprise a small population of the fibroblastic cells that surround the portal vein to maintain integrity of portal tract. They were first described as "mesenchymal cells not related to sinusoids," and since then have been called "periductular fibroblasts" or portal/periportal mesenchymal cells" (11) and implicated by association in the pathogenesis of cholestatic liver injury. In

## Significance

**Liver resident activated hepatic stellate cells (aHSCs), and activated portal fibroblasts (aPFs) are the major source of the fibrous scar in the liver. aPFs have been implicated in liver fibrosis caused by cholestatic liver injury, whereas fibrosis in hepatotoxic liver injury is attributed to aHSCs. However, the contribution of aPFs to cholestatic fibrosis is not well characterized because of difficulties in cell purification and the lack of identified aPF-specific markers. We have developed a novel flow cytometry-based method of aPFs purification from the nonparenchymal cell fraction of collagen-α1(I)-GFP mice and have identified potential aPF-specific markers. The goal of this study is to determine whether aPFs contribute to cholestatic liver fibrosis and identify the mechanism(s) of their activation.**

Author contributions: K.I., C.J., M.Z., D.A.B., and T.K. designed research; K.I., C.J., M.Z., M.C., T.J.M.-M., T.J.P., X.L., J.X., P.W., Y.-H.P., F.M., L.A.M., and T.K. performed research; M.A., A.F.H., T.I., C.K.G., and D.A.B. contributed new reagents/analytic tools; K.I., C.J., M.Z., M.C., T.J.M.-M., T.J.P., X.L., J.X., Y.-H.P., F.M., M.A., and C.K.G. analyzed data; and D.A.B. and T.K. wrote the paper.

The authors declare no conflict of interest.

*This Direct Submission article had a prearranged editor.

Freely available online through the PNAS open access option.

[1]K.I., C.J., and M.Z. contributed equally to this work.

[2]To whom correspondence should be addressed. Email: tkisseleva@ucsd.edu.

This article contains supporting information online at www.pnas.org/lookup/suppl/doi:10.1073/pnas.1400062111/-/DCSupplemental.

response to chronic injury, portal fibroblasts may proliferate, differentiate into α-SMA–expressing myofibroblasts, and synthesize extracellular matrix (11–14).

The contribution of portal fibroblasts (PFs) to liver fibrosis of different etiologies is not well understood, mainly because of difficulties in isolating PFs and myofibroblasts. The most widely used method of PF isolation from rats is based on liver perfusion with enzymatic digestion followed by size selection (15). Cell outgrowth from dissected bile segments is still used to isolate mouse PFs, and after 10–14 d in culture, PFs undergo progressive myofibroblastic activation (16). The disadvantage of this technique is that it requires multiple passaging and prolong culturing (11). A more physiological method of PF culturing in a precision-cut liver slice is designed to maintain cell–cell and cell–matrix interactions and mimic natural microenvironment of PFs, but it does not enable the study of purified PFs (17). Therefore, only a few markers of PFs are available to identify PFs in the myofibroblast population, including gremlin, Thy1, fibulin 2, interleukin 6 (IL-6), elastin, the ecto-AT-Pase nucleoside triphosphate diphosphohydrolase-2 (NTPD2), and coffilin 1. In addition, the lack of desmin, cytoglobin, α2-macroglobulin, neural proteins (GFAP, p75, synaptophysin), and lipid droplets distinguishes PFs from HSCs (1, 17–21).

Our study uses transgenic reporter mice and new flow cytometry protocols to identify the origin of myofibroblasts and quantify their numbers in two murine models of chronic liver injury (BDL and $CCl_4$). Our study demonstrates that the origin of the myofibroblasts is determined by the type of liver injury. As previously reported using other methodologies, HSCs are the major source of myofibroblasts in $CCl_4$ liver injury. In contrast, most of the myofibroblasts at the onset of BDL-induced liver injury originate from activated PFs (aPFs).

## Results

**BDL- and $CCl_4$-Induced Liver Fibrosis Is Associated with Activation of Myofibroblasts in Mice.** To study activation of hepatic myofibroblasts, Col-GFP mice expressing GFP under control of collagen α1(I) promoter/enhancer (22) were subjected to BDL (20 d) or $CCl_4$ (1.5 mo) liver injury. Upon activation, hepatic myofibroblasts in these mice are visualized by GFP expression. Development of liver fibrosis was confirmed in Col-GFP mice by hydroxyproline content, Sirius Red staining (Fig. 1 *A* and *B*) and correlated with increased collagen-α1(I) (fold increase 6.1 ± 0.3 and 7.6 ± 0.4 in BDL- and $CCl_4$-treated vs. control mice) and α-SMA mRNA expression (fold increase 4.2 ± 0.2 and 6.1 ± 0.7 vs. control mice, respectively; Fig. 1*B*). Development of liver fibrosis was also associated with activation of myofibroblasts, demonstrated by Col-GFP expression (6.5 ± 0.4% and 7.8 ± 0.5% of $GFP^+$ area in BDL- and $CCl_4$-treated vs. 0.3 ± 0.03% in control mice) and α-SMA expression (Fig. 1*B*). Thus, BDL and $CCl_4$ induced comparable levels of fibrosis and activation of myofibroblasts in the liver, sufficient to isolate $GFP^+$ myofibroblasts and determine their composition in response to two different injuries.

**Isolation of Myofibroblasts.** The reporter Col-GFP mice (22) have been extensively characterized and are widely used to visualize activated myofibroblasts in fibrotic liver, lungs, kidneys, and skin (3–5, 8, 23–36). Expression of GFP in these mice closely correlates with expression of collagen type I protein in hepatic myofibroblasts but is not expressed in endothelial, epithelial, or other cell types (37–39). Using Col-GFP mice we have demonstrated that activated hepatic stellate cells (aHSCs) ($GFP^+$, vitamin $A^+$, $Desmin^+$ cells) comprise >92% of myofibroblasts in response to $CCl_4$-induced or alcohol-induced fibrosis (1, 40).

**Analysis of Activated Myofibroblasts by Flow Cytometry.** Our strategy to determine the composition of hepatic myofibroblasts is

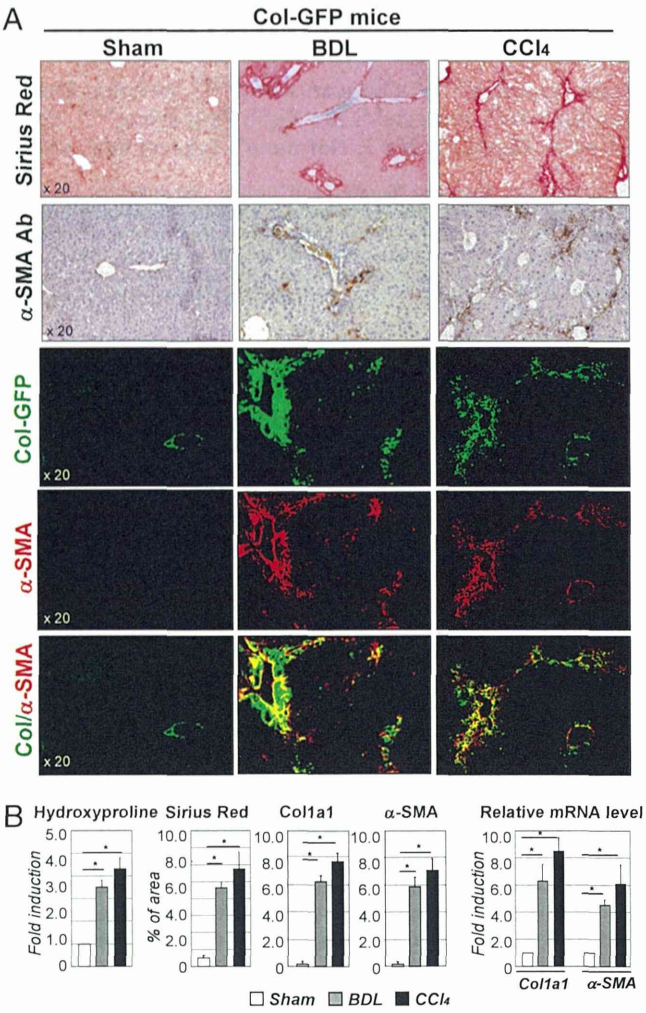


**Fig. 1.** Development of liver fibrosis in Col-GFP mice in response to BDL and $CCl_4$. (*A*) $CCl_4$-treated and BDL-operated mice (but not sham mice, 8-wk-old, $n = 10$ per group) developed liver fibrosis, as shown by Sirius Red staining, fluorescent microscopy for collagen-GFP, and staining for α-SMA (20× objective). (*B*) Fibrosis was assessed by hydroxyproline and Sirius Red (positive area) content and by mRNA levels of fibrogenic genes (Col and α-SMA) in all groups of mice is shown, $^*P < 0.003$; $^{**}P < 0.001$.

based on characterization of $GFP^+$ cells in nonparenchymal liver fractions of BDL- and $CCl_4$-treated Col-GFP mice (which contains all $Col1a1^+$ and $\alpha\text{-}SMA^+$ myofibroblasts; for details, see Fig. S1*A*) (22). Although collagen-α1(I)-GFP is expressed in all activated myofibroblasts (40, 41), expression of vitamin A (Vit.A) droplets in the liver is solely attributed to HSCs (1) (Fig. 2*A*). The cell fate mapping of HSCs [using $GFAP^{Cre} \times Rosa26^{flox\text{-}TmRed\text{-}Stop\text{-}flox\text{-}GFP}$ mice (40); Fig. S1 *B* and *C*] demonstrated that although HSCs down-regulate vitamin A upon activation (aHSCs), vitamin A is still detected in all aHSCs by flow cytometry (autofluorescent signal of vitamin A; Fig. S1*D*). We used flow cytometry to quantify the contribution of aHSCs ($GFP^+Vit.A^+$) and myofibroblasts of other origins ($GFP^+Vit.A^-$) in BDL and $CCl_4$ injury (Fig. 2*B*). As expected, activation of hepatic myofibroblasts ($GFP^+$ cells, 100%) was observed only in injured livers (Fig. 2*B*). $CCl_4$-activated myofibroblasts contained 87 ± 6% $GFP^+Vit.A^+$ and 13 ± 3% $GFP^+Vit.A^-$ cells. In contrast, the nonparenchymal fraction from BDL (20 d) mice consisted of 56 ± 4% $GFP^+Vit.A^+$ and 42 ± 5% $GFP^+Vit.A^-$ myofibroblasts, suggesting that the composition of $GFP^+$

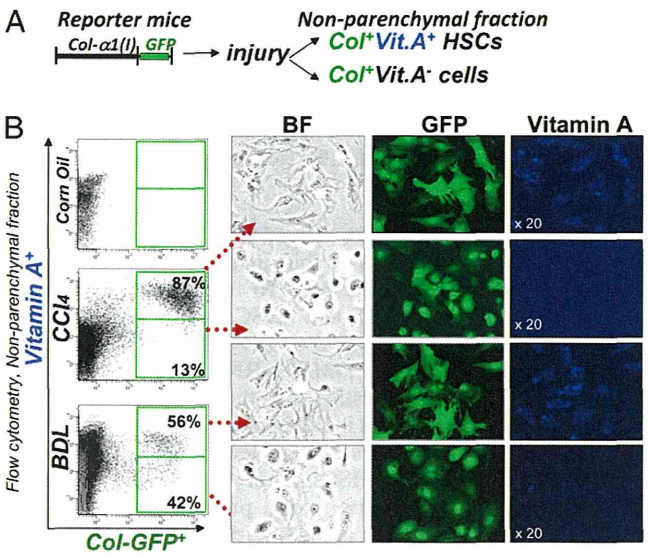


C

| GFP⁺ Myofibroblasts, % | | Vit.A⁺ | Vit.A⁻ |
|---|---|---|---|
| $CCl_4$ | 5 days | 79 ± 3.8 | 5 ± 2.0 |
| $CCl_4$ | 14 days | 88 ± 4.0 | 10 ± 3.6 |
| $CCl_4$ | 1.5 mo | 87 ± 5.2 | 13 ± 2.0 |
| BDL | 5 days | 18 ± 7 | 73 ± 5 |
| BDL | 17 days | 45 ± 3 | 53 ± 4 |
| BDL | 20 days | 56 ± 4 | 46 ± 3 |

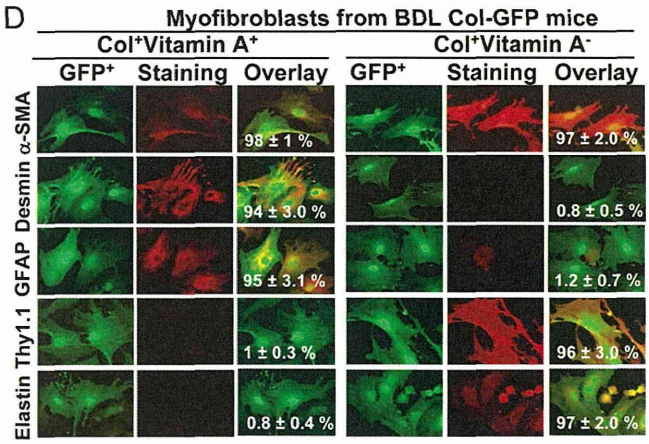


E

| GFP⁺ Myofibroblasts, % | | HSCs | aPFs | Others |
|---|---|---|---|---|
| $CCl_4$ | 1.5 mo | 83 ± 5.2 | 13 ± 2.0 | 4 ± 2.4 |
| BDL | 5 day | 18 ± 7 | 73 ± 5 | 3 ± 2 |
| BDL | 17 days | 47 ± 3 | 49 ± 6 | 4 ± 0.8 |
| BDL | 20 days | 51 ± 4 | 43 ± 3 | 3 ± 1.4 |

**Fig. 2.** Detection, quantification, and isolation of liver myofibroblasts. (*A*) Strategy to analyze myofibroblasts by flow cytometry: Collagen type I-expressing myofibroblasts were identified in nonparenchymal fraction by GFP expression and further fractionated to Vit.A$^+$ and Vit.A$^-$ cells. (*B*) FACS analysis of nonparenchymal fraction from untreated and BDL-, and $CCl_4$-treated Col-GFP mice: GFP$^+$ cells were detected by argon laser at 488 nm wavelength, and Vit.A$^+$ cells were detected by violet laser at 405 nm wavelength. Representative dot plots are shown, $P < 0.03$. GFP$^+$Vit.A$^+$ and GFP$^+$Vit.A$^-$ cells were sort purified and analyzed by light and fluorescent microscopy for GFP and Vitamin A expression (UV laser, 20× objective). (*C*) Flow cytometry-based quantification of GFP$^+$ myofibroblasts. Expression of vitamin A in GFP$^+$ cells was analyzed in nonparenchymal fraction of Col-GFP mice at different time points ($n = 6$ per time point) of $CCl_4$ and BDL, $P < 0.01$. (*D*) Immunophenotyping of GFP$^+$ myofibroblasts isolated from BDL mice. GFP$^+$Vit.A$^+$ and GFP$^+$Vit.A$^-$ fractions were sort purified from Col-GFP mice ($n = 6$) after BDL (20 d). Expression of myofibroblast marker (α-SMA), HSC markers (desmin, GFAP, CD146), and PF markers (elastin, Thy1) were analyzed by immunocytochemistry using specific antibodies or isotype matched controls (40× objective). GFP$^+$Vit.A$^+$ and GFP$^+$Vit.A$^-$ cells were identified as aHSCs and aPFs, respectively. For each fraction, the percent of positively stained cells is calculated (compared with total cells, 100%, $P < 0.05$). (*E*) Quantification of GFP$^+$Vit.A$^+$ and GFP$^+$Vit.A$^-$ fractions is based on expression of HSC- and PF-specific markers in GFP$^+$ myofibroblasts (100%) as detected by immunocytochemistry, $P < 0.05$.

myofibroblasts varies depending on the etiology of liver fibrosis. GFP$^+$Vit.A$^+$ and GFP$^+$Vit.A$^-$ cells were sort purified and plated (Fig. 2*B*). Expression of GFP was confirmed in both fractions by fluorescent microscopy, whereas expression of Vit.A$^+$ droplets was detected only in GFP$^+$Vit.A$^+$ cells.

**Activation of HSCs Differs in BDL- and $CCl_4$-Induced Liver Injury.** Analysis of all GFP$^+$ myofibroblasts (100%) demonstrated that GFP$^+$Vit.A$^+$ aHSCs are the major source of activated myofibroblasts in response to $CCl_4$ liver injury (Fig. 2*B*). Even at earlier time points of $CCl_4$ treatment, 79 ± 3% (at 5 d) and 88 ± 4% (at 14 d) of the myofibroblasts were GFP$^+$Vit.A$^+$ HSCs (Fig. S2*A*). In contrast, BDL activated fewer HSCs (Fig. S2*B*). After 5 d of BDL, GFP$^+$ myofibroblasts were mainly composed by GFP$^+$ Vit.A$^-$ cells (73 ± 5%), whereas GFP$^+$Vit.A$^+$ aHSCs represented only 18 ± 7% of GFP$^+$ cells. After BDL (17 d), GFP$^+$ myofibroblasts consisted of 53 ± 4% of GFP$^+$Vit.A$^-$ cells and 45 ± 3% of GFP$^+$Vit.A$^+$ aHSCs, suggesting that activation of HSCs in BDL follows the induction of GFP$^+$Vit.A$^-$ myofibroblasts. Flow cytomery-based statistical analysis of the number of Vit.A$^+$ and Vit.A$^-$ myofibroblasts in response to BDL and $CCl_4$ is summarized in Fig. 2*C*.

**GFP$^+$Vit.A$^+$ Myofibroblast Originate from HSCs, Whereas GFP$^+$Vit.A$^-$ Derive Predominantly from aPFs.** Sort-purified GFP$^+$Vit.A$^-$ and GFP$^+$Vit.A$^+$ myofibroblasts were characterized by immunostaining for specific markers. As expected, all GFP$^+$ cells expressed the myofibroblast marker α-SMA, demonstrating that only myofibroblasts express type I collagen in liver fibrosis. BDL-activated GFP$^+$Vit.A$^+$ myofibroblasts expressed the typical HSC markers GFAP (94 ± 2.6%), desmin (98 ± 2%), and mesenchymal marker CD146 (87 ± 3.0%), confirming that the GFP$^+$ Vit.A$^+$ fraction consists solely of aHSCs (Fig. 2*D*). As expected, $CCl_4$-induced GFP$^+$Vit.A$^+$ myofibroblasts were aHSCs (Fig. S3*A*). In contrast, GFP$^+$Vit.A$^-$ myofibroblasts stained positive for the established portal fibroblast markers Thy1 (93 ± 4.0%) and elastin (86 ± 3.4%), but lacked markers of HSCs (GFAP, Desmin, CD146; Fig. 2*D*) and myeloid cells (CD11b, F4/80, CD68; Fig. S3*B*). Only a small number of GFP$^+$Vit.A$^-$ cells expressed fibrocyte-like markers CD45 (3.1 ± 0.1%) and CD11b (2.4 ± 0.3%; Fig. S3*B*), suggesting that GFP$^+$Vit.A$^-$ fraction predominantly (95 ± 4%) contains aPFs, and that less than 4 ± 1% of myofibroblasts originate from other sources (e.g., fibrocytes and BM derived mesenchymal progenitors). Immunocytochemistry-based analysis of myofibroblast composition in response to both BDL and $CCl_4$ is summarized in Fig. 2*E*.

**Gene Expression Profile Distinguishes BDL-Derived aPFs from $CCl_4$-aHSCs and BDL-aHSCs.** The gene expression profile of BDL-aPFs was compared with BDL-aHSCs and $CCl_4$-aHSCs (Fig. 3*A*). Using a threshold defining confident detection of gene expression, we confirmed that aPFs exhibited a myofibroblast-like phenotype, sharing mRNA expression of 8,981 genes with aHSCs. These genes included *Col1a1, Col1a2, Col2a1, TIMP-1, Spp1, TGFβ-RI,* and *Vimentin* (Fig. 3*C*) and were induced in aPFs to a level comparable to BDL- and $CCl_4$-aHSCs. As expected, GFAP and Bambi mRNAs were highly expressed in

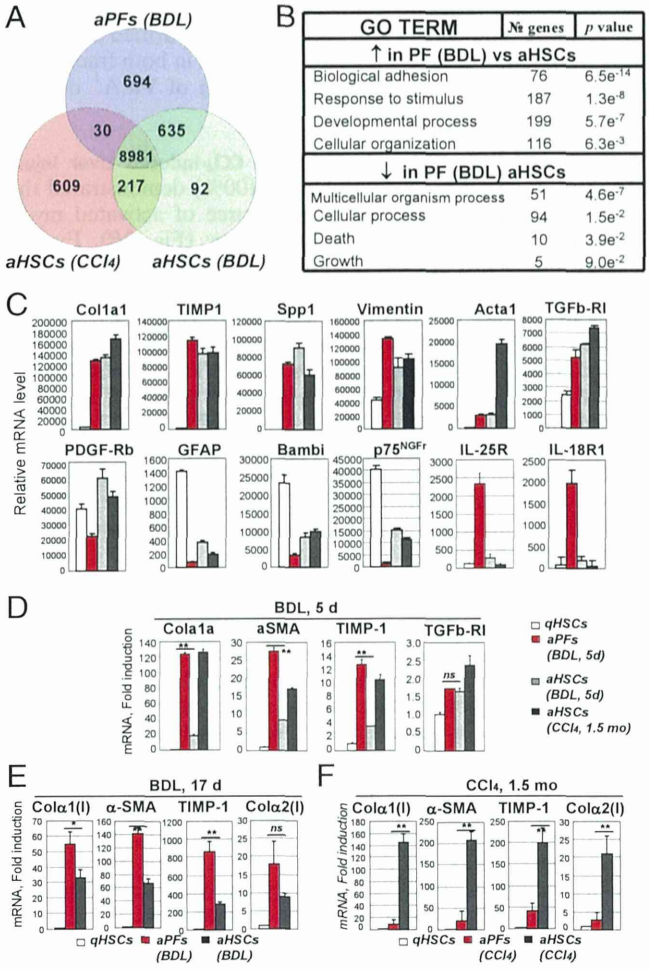


**Fig. 3.** Characterization of aPFs and aHSCs. (*A*) BDL (20 d) GFP$^+$Vit.A$^-$ aPFs and GFP$^+$Vit.A$^+$ aHSCs were analyzed by the whole mouse genome microarray, and their gene expression profile was compared with that in $CCl_4$-activated GFP$^+$Vit.A$^+$ HSCs. Venn diagrams of the cell group-enriched genes that exhibited more than a twofold up-regulation compared with other groups. (*B*) GO TERM: demonstrates the signaling pathways that were up-regulated or down-regulated in BDL-aPFs versus BDL- or $CCl_4$-aHSCs. (*C*) Expression of selected genes in qHSCs, BDL-aHSCs and BDL-aPFs, and $CCl_4$-aHSCs. The results are relative mRNA level (average of normalized values/multiple probes/per gene) obtained by Agilant microarray, $P < 0.001$. (*D*) Expression of fibrogenic genes was analyzed by RT-PCR in BDL- (5 d) aPFs and BDL-aHSCs, isolated from the same mice ($n = 6$), and compared with that in qHSCs-aHSCs and $CCl_4$ (1.5 mo)-aHSCs. The data are shown as fold induction compared with qHSCs, $^{**}P < 0.02$ is shown for BDL-aPFs and BDL-aHSCs; ns is not significant. (*E*) Expression of fibrogenic genes was analyzed in BDL (17 d)-aPFs and BDL-aHSCs (isolated from the same mice, $n = 6$) by RT-PCR vs. qHSCs. The data are shown as fold induction compared with qHSCs, $^{*}P < 0.05$; $^{**}P < 0.01$; ns, nonsignificant. (*F*) Similarly, $CCl_4$- (1.5 mo)aPFs and $CCl_4$-aHSCs, isolated from the same mice ($n = 4$) were analyzed by RT-PCR. The data are shown as fold induction over qHSCs, $^{*}P < 0.05$; $^{**}P < 0.01$. The data in *D–F* represent at least three independent experiments.

qHSCs, whereas *PDGF-Rb* was up-regulated in aHSCs. Meanwhile, the highest expression of *Acta1* was detected in $CCl_4$-aHSCs (Fig. 3*C*). aPFs up-regulated an additional 694 unique genes (Fig. 3*A*). This set of genes was enriched in Gene Ontology biological process annotations linked to biological adhesion, response to stimulus, developmental process and cellular organization (Fig. 3*B*), locomotion, focal adhesion, cell adhesion molecules, regulation of actin cytoskeleton, and were associated with the induction of the profibrogenic Wnt signaling pathway (Fig. S4). Furthermore, aPFs up-regulated expression of IL-18R, IL-25R (Fig. 3*C*), and other genes that distinguish them from aHSCs (Table 1, discussed below). Interestingly, BDL-aHSCs differentially expressed only 92 genes and shared more similarity with aPFs (635 genes) than with $CCl_4$-aHSCs (217 genes; Fig. 3*A*), suggesting that in response to cholestatic liver injury, aHSCs may mimic the phenotype of aPFs (for comparison of BDL- and $CCl_4$-aHSCs, see Fig. S5).

**PFs Are Activated in Early BDL-Induced Liver Injury.** Our data indicate that aPFs and aHSCs exhibit similar level of activation in response to BDL (20 d; Fig. 3*C*). To further characterize the fibrogenic properties of aPF and aHSC, earlier time points of BDL were examined. After 5 d of BDL (Fig. 3*D*), expression levels of *Col1a1*, *aSMA*, and *TIMP1* mRNA were much higher in aPFs than in aHSCs, suggesting that the activation of PF precedes the activation of HSCs in BDL injury. For example, *Col1a1* was 120-fold induced in aPFs over the level in qHSCs, compared with 20-fold induction in aHSCs. After 17 d of BDL (Fig. 3*E*), activation of HSCs became more prominent (i.e., *Col1a1* mRNA: 33-fold induction in aHSCs, vs. 55 in aPFs). Meanwhile, $CCl_4$-aPFs exhibited a much lower level of *Col1a1* mRNA than $CCl_4$-aHSCs (fold induction 20 and 160, respectively; Fig. 3*F*), demonstrating that PFs are only minor contributors to toxic $CCl_4$-induced liver injury. These data are in concordance with our previous results obtained by flow cytometry (Fig. 2) and

**Table 1. Expression of signature genes distinguishes BDL-aPFs from BDL- and $CCl_4$-aHSCs**

| Maximum induction (up-regulation) in aPF (BDL, 20 d) | Fold |
|---|---|
| *Calcitonin α (Calca)* | 66 |
| *Glycoprotein m6a (Gpm6a)* | 35 |
| *Uroplakin 1β* | 28 |
| *Basonuclin 1 (Bnc1)* | 24 |
| *Mesothelin (msln)* | 24 |
| *Frizzled-related protein 4 (Sfrp4)* | 21 |
| *Cyp2s1* | 20 |
| *Proteoglycan 4 (Prg4)* | 18 |
| *Asporin (aspn)* | 18 |
| *Mucin 16 (Muc16)* | 16 |
| *IL-18R1* | 14 |
| *Myosin light peptide7 (Myl7)* | 14 |
| *Vitrin (Vit)* | 12 |
| *Glipican 3 (Gpc3)* | 12 |
| *CD200* | 11 |
| *Apolipoprotein D (ApoD)* | 10 |
| *IL-25R* | 9.7 |
| *Dermokin (Dmkn)* | 9.3 |
| *Vanin (Vnn1)* | 8.5 |
| *Thrombospondin 4 (Thbs4)* | 7.0 |
| *Integrin β4 (Itgb4)* | 6.5 |
| *CD55* | 5.6 |
| *Gremlin 1 (Grem1)* | 4.8 |
| *NTPD2* | 4.6 |
| *PDGFc* | 4.6 |
| *Fibulin 2 (Fbln2)* | 4.4 |
| *CD9* | 3.1 |
| *Elastin (Eln)* | 2.3 |
| *Thy1 (CD90)* | 1.8 |
| *Cytoglobin* | 0.6 |

Using the whole mouse genome microarray, expression of signature genes was determined for BDL-aPFs. Expression of genes previously identified as PF-specific (underlined) was confirmed. Fold induction (compared with the highest value observed in BDL- or $CCl_4$-aHSCs) is shown for each gene. Full list of genes is shown in Fig. S7.

demonstrate that there is a correlation between increased number of BDL-aPFs and the level of their activation.

**Functional Properties of BDL-Derived aPFs Differ from aHSCs.** Previous studies have proposed differences in aPFs and aHSCs that underlie fibrogenesis of different etiologies (42). Therefore, we assessed how aPFs and aHSCs responded to fibrogenic stimuli in vitro. As expected, the fibrogenic cytokine TGF-β1 had similar effects on aPF and aHSC (Fig. 4*A*). However, aPFs were unresponsive to the known HSC agonists PDGF and NGF (demonstrated by mRNA expression of target genes *CyclinD1*; *Bax*, *Bid*, *Bim*, *Bcl-2*, and *Bcl-xl*, respectively). Despite high expression of IL-18R, treatment of aPFs with IL-18 (100 ng/mL; 8 h) did not induce expression of tested IL-18 target genes (*MMP3, MMP8*, and *MMP13, Cox-2, iNOS, IL-6*). Meanwhile, only PFs responded to the bile acid TCA, with increased *Col1a1* mRNA expression (>2.2-fold induction over control aPFs), suggesting that TCA may directly mediate PF activation (Fig. 4*B*). Furthermore, aPFs responded to IL-25 stimulation by induction of IL-13 [similar to IL-13 induction by IL-25–treated macrophages (43) and fibroblasts (44)]. Although IL-13 is implicated in HSC activation, and IL-13 levels are up-regulated in patients with liver cirrhosis (3, 4, 27), the role of IL-13 in cholestatic liver injury has not been well defined. We hypothesize that IL-25–mediated IL-13 production by BDL-aPFs may stimulate activation of HSCs. To assess the effect of aPF-produced IL-13 on HSCs, qHSCs were incubated in the presence of IL-13. As we predicted (45), IL-13 increased *CTCF* (after 4 h) mRNA expression, and also induced up-regulation of *Col1a1*, *aSMA*, *TIMP1*, and mRNA (after 24 h) in HSCs (Fig. 4*C*), suggesting that aPFs may locally facilitate HSC activation via production of IL-13. A more detailed analysis (Fig. 4*D*) demonstrated that stimulation of HSCs with IL-13 causes up-regulation of IL-13Ra2 expression (but not IL-13Ra1 or IL-4) and transcription of IL-13 target genes *Tenascin-C* and *Eotaxin* (46, 47). Because IL-13–treated HSCs did not express IL-13 or IL-6, we concluded that IL-13 directly mediated HSC activation, and this effect was associated with phosphorylation of ERK1/2 (which is completely blocked by ERK inhibitor U0126; Fig. 4*E*) and activation of the p38 and Smad1/5 signaling pathways. Similar results were obtained in human primary HSCs. hIL-13 induced a dose-dependent secretion of CCL11/eotaxin (Fig. S6*A*) in hHSCs. In a separate experiment, hIL-13 alone (or in combination with TGF-β1) mediated an increase in IL-13Ra2, *Tenascin C*, *Col1a1*, *Col3a1*, *fibronectin*, and *LoxL2* genes (Fig. S6*B*). In turn, TGF-β1 and serum stimulation did not result in IL-13 secretion by hHSCs (Fig. S6*C*), suggesting that aPFs may serve as a source of IL-13 in liver fibrosis.

**Expression of Novel Markers Distinguishes BDL-Derived aPFs from BDL-aHSCs and $CCl_4$-aHSCs.** To further distinguish aPFs from aHSCs and other myofibroblasts, we interrogated the whole mouse genome microarray to determine "signature genes" for aPFs (Table 1). In concordance with previous studies, we confirmed that aPFs lack expression of cytoglobin (an HSC marker), but express Thy1, elastin, Gremlin 1, Fibulin 2, and NTPD2 mRNAs (the markers that have been reported to discriminate between aPFs and aHSCs) (2, 11, 17–21). However, expression of cofilin-1 (21) distinguished aPFs from $CCl_4$-aHSCs, but not from BDL-aHSCs, which limits the usefulness of this marker. Furthermore, aPFs uniquely expressed calcitonin α (fold induction >48 over the highest value in BDL-aHSCs or $CCl_4$-aHSCs), mesothelin (>28), uroplakin 1β (>22), basonuclin 1 (>18), asporin (>14), proteoglycan 4 (>14), glipican 3 (>12), and CD200 (>11) mRNA (Fig. S7). Up-regulation of these genes specifically in aPFs [but not in quiescent or aHSCs, endothelial cells, Kupffer cells, and hepatocytes (Fig. 5*A* and Fig. S8*A*) or BDL-activated cholangiocytes (Fig. 5*A* and Fig. S8*C*)] was confirmed by RT-PCR and immunohistochemistry, suggesting that these genes may serve as potential novel markers of aPFs. Some of these genes (including *basonuclin 1, glycoprotein m6a, uroplakin 3b and 1b, mesothelin, IL-18R, calcitonin-related peptides,* and *vitrin*) were reported as signature genes of murine hepatic mesothelial (48) and epicardial cells (49) (Fig. S7), supporting the theory that PFs originate from mesothelial cells (50, 51).

The role of most of these genes in liver fibrosis has not been evaluated, with the exception of calcitonin α and mesothelin. Calcitonin α, a calcium metabolism regulating hormone, was implicated in pathogenesis of cholestatic injury, and mice devoid of calcitonin α are more resistant to BDL-induced liver fibrosis (52). In turn, mesothelin, a glycosylphosphatidylinositol-linked glycoprotein, is expressed in hepatic mesothelial cells and malignant mesotheliomas (53) and mediates intracellular adhesion and metastatic spread (54). Mesothelin knockout mice are viable and exhibit no obvious abnormalities (55). Expression of mesothelin was detected only in isolated aPFs but not in other cellular fractions (Fig. 5*A*).

**Expression of Mesothelin Is Up-Regulated in aPFs in Response to Injury.** We examined the expression of mesothelin in isolated aPFs and aHSCs. Unlike $GFP^+GFAP^+$ aHSCs, $GFP^+$ aPFs expressed mesothelin (97 ± 1.7%). $Mesothelin^+$ aPFs coexpressed elastin (detected with TE-7 Ab) and Thy1, and immunostaining with mesothelin colocalized with $Elastin^+Thy1^+$ aPFs (Fig. 5*B* and Fig. S8*B*). Next, expression of mesothelin was evaluated in livers of BDL- and $CCl_4$-injured mice (Fig. 5*C* and Fig. S8*B*). In concordance with our previous findings, very few $mesothelin^+$ cells were detected in $CCl_4$-injured livers. In contrast, mesothelin was highly expressed in livers from BDL-injured mice, with an expression pattern similar to the other PF markers Thy1 and elastin (Fig. S8 *B* and *C*). In support of our findings, expression of mesothelin mRNA was also detected in laser capture microdissected portal areas from BDL (20 d)-treated mice but not from $CCl_4$-treated mice (Fig. 5*D*). In addition, mesothelin was not expressed in sham-operated mice, suggesting that mesothelin identifies the aPF phenotype.

## Discussion

Our study was designed to determine the origin of hepatic myofibroblasts activated in response to chronic injury of two different etiologies. We demonstrate that hepatotoxic ($CCl_4$) and cholestatic (BDL) liver injuries activate distinct subsets of fibrogenic myofibroblasts. Thus, $CCl_4$ activates preferentially aHSCs, whereas BDL initially preferentially aPFs. We developed a reliable method of isolation and quantification of hepatic myofibroblast fractions by using flow cytometry. Based on the distinctive expression of Vitamin A and GFAP in HSCs and Thy1 and elastin in PFs, this study establishes cell sorting as a robust method to purify distinct populations of myofibroblasts in mice, providing a nonbiased approach to purify and characterize all myofibroblasts. By demonstrating that HSCs are the major source of myofibroblasts in hepatotoxic liver injury ($CCl_4$), we confirmed the previous cell fate mapping studies that used GFAP-Cre (56, 57), PDGFRb-Cre (58), and Lrat-Cre (59).

In contrast to $CCl_4$-induced injury, our study demonstrates that PFs rapidly activate at the onset of cholestatic injury and up-regulate fibrogenic genes. Furthermore, early activation of PFs during BDL injury may affect HSCs, and BDL-aHSCs exhibit more similarity to aPFs than to $CCl_4$-aHSCs. Gene expression profiling demonstrated novel signature genes for aPFs. According to cell fate mapping, PFs originate from the mesothelium (51, 60), and our data suggest that aPFs share similarity in signature gene expression with other cells of mesothelial origin. One of these genes, mesothelin, is highly induced specifically in aPFs in response to BDL injury, suggesting that mesothelin may become a new target for antifibrotic therapy.